Progress in the synthesis of 2D black phosphorus beyond exfoliation

*Yuqian Zhao[1], Zehan Wu[1,2], Zhaoying Dang[1], Jianhua Hao[1,2]**

[1]Department of Applied Physics, The Hong Kong Polytechnic University, Hung Hom, Hong Kong, P.R. China

[2]The Hong Kong Polytechnic University Shenzhen Research Institute, Shenzhen 518057, P. R. China

*Corresponding Author: E-mail: jh.hao@polyu.edu.hk

Abstract

A considerable number of recent researches have focused on two-dimensional (2D) black phosphorus (BP) since it was successfully prepared through mechanical exfoliation in 2014. After scaling down, BP with atomistic thickness shows fascinating semiconducting features with layer-dependent direct bandgap and high carrier mobility. The synthesis of high-quality few-layer BP thin films is critical to investigate their distinctive crystal structure, fundamental characteristics, as well as the potential applications in electronics, biomedicine, energy storage, photonics and optoelectronics. Therefore, this review provides an overview of mono- and few-layer BP topic in the synthesis methods beyond exfoliation, including thinning treatments accompanied to exfoliation, conversion from red phosphorus to BP and direct growth techniques. We summarize various attempts to control the BP sample's thickness and lateral dimensions during the synthesis. Furthermore, we discuss the current challenges and perspectives of large-scale growth of ultrathin BP which has been a bottleneck hindering wafer-

scale device's development in this field. We hope to provide an insight into exploring some potential approaches practicable to synthesize high quality BP thin films utilized for developing high-performance nano-electronics and photonics, which may accelerate the progress of 2D BP toward real applications.

1. Introduction

Since the discovery of monolayer graphene mechanically exfoliated from bulk graphite in 2004[1], two-dimensional (2D) nanomaterials have recently generated extensive research interest due to their widespread potential applications in a variety of fields, including flexible devices[2], sensors[3], and optics[4]. Mechanical exfoliation is the most frequently employed top-down approach for preparing monolayer and few-layer nanoflakes at the initial stage of the emerging 2D materials.[5] As multilayer 2D materials with high crystal quality can be conventionally separated from the single-crystalline bulks by applying the Scotch tape isolation, the fundamental characteristics of the 2D materials can be greatly retained and investigated. However, this approach is not advantageous for large-scale fabrication of 2D thin films, in which precise control over the film thickness (number of layers) and lateral dimension is difficult due to the limitation of this approach. Therefore, various synthetic techniques beyond mechanical exfoliation and other bottom-up approaches were investigated to aim at developing high-quality, uniform, and large-scale 2D materials.[6-8]

Over a century ago, BP was initially discovered as an allotrope of the phosphorus family with semiconducting characteristic.[9] In 2014, 2D black phosphorus (BP) and phosphorene (monolayer BP) were exfoliated with scotch tape approach and they have recently emerged as a promising elemental alternative to graphene.[10] Despite its high charge carrier mobility, graphene is unable to work as a semiconductor due to the lack of a bandgap in its

electronic structure, restricting its potential in a wide range of applications, particularly in some logic electronic and optoelectronic devices.[11] Transition metal dichalcogenides (TMDs), which is another important member of the 2D materials family, have also piqued enormous interests owing to their substantial band gap and semiconducting characteristic.[12] Nevertheless, the large band gap of TMDs only covers partial visible range in the electromagnetic spectrum, severely limiting their broad applications.[13] In comparison, 2D BP not only possesses a moderate and tunable band gap between graphene (0 eV) [14] and TMDs (1.0 eV-2.0 eV)[15,16], which covers a broad spectrum ranging from visible to mid-infrared light. The scaling down of BP also offers a thickness-mediated direct band gap[17], remarkable hole-dominated carrier mobility[18], and notable on/off ratio[10]. Furthermore, as the orthorhombic lattice structure of BP is lack of symmetry, the induced in-plane anisotropy allows the crystal orientation to modulate the optical and electrical characteristics of 2D BP.[19,20] Owing to the various aspects of fascinating properties, BP has become one of the most attractive and frequently researched materials among the 2D family.[21] These characteristics also make BP a unique candidate for device development, including optoelectronic[22], energy storage[23], biomedical[24], and photonics applications[25]. Design and fabrication of high-performance BP-based devices with diverse applications have been extensively carried out via multiple manipulation strategies including interface and defects modification[26], bandgap engineering[27], and formation of stacked heterostructures[28]. Although BP-based devices have shown attractive application potential, unfortunately it is still one of the few 2D materials that exhibits serious difficulty in scale-up and controllable preparation of its few-layer large-area thin films, which severely hampered the future practical applications based on 2D BP.

So far, there is no specific review emphasizing on the topic of 2D BP synthesis methods beyond exfoliation, instead most of the published reviews have been focusing on the

passivation and applications of BP. To promote BP's integration in terms of reliability standards, the issue of the lack of an efficient bottom-up technique for synthesizing thin layers at the wafer scale also needs to be addressed. In this review, we will highlight and summarize the recent works regarding the synthesis methods beyond exfoliation for mono- and few-layer BP thin films, as well as the attempts to regulate their thickness and lateral size accurately. The intention of this review is to provide essential information for the further research on the large-scale 2D BP and to guide the exploration of the viable techniques that are applicable for synthesizing high-quality 2D BP, with the aim of contributing to its research and development.

2. Fundamental structure and characteristics of BP

Red phosphorus (RP), white phosphorus (WP), purple phosphorus (PP), and BP are the most common allotropes of phosphorus, which is one of the most prevalent elements on the earth. The crystal structure of BP has several forms, including orthorhombic, simple cubic, orthogonal, diamond and nanorod. Bachhuber et al. used quantum mechanical simulations to demonstrate that the van der Waals (vdW) force between layers is the most critical attractive force in determining the order of stability in all existing phosphorus allotropes, as the vdW force connects the layers together, resulting in the formation of bulk BP crystal. [29] Among all phosphorus allotropes, orthorhombic BP is the most thermodynamically stable structure.[30]

As shown in Figure 1a, the atoms in the P_4 molecule of WP are positioned at the corners of a tetrahedron, with each phosphorus atom is singly bonded to the each other. The P_4 structure of WP has six P-P single bonds and four lone pairs electrons. Unlike the 90° angle formed by pure 3p orbitals, the angle between the P-P-P bond is 60.31°.[31] Therefore, the tetrahedral arrangement is stabilized by arc-like bonds, resulting in ring strain and instability.[32] In comparison, the P_4 molecules are connected to form BP layers in monolayer BP (also known

as phosphorene). The individual P_4 bonds are broken by sp^3 hybridization, leading to the formation of two distinct bond angles 99.48° and 103.37° (presented in Figure 1b). As a result, the stability of the BP is improved when these angles approach the optimal tetragonal structural angle of 109.5°.

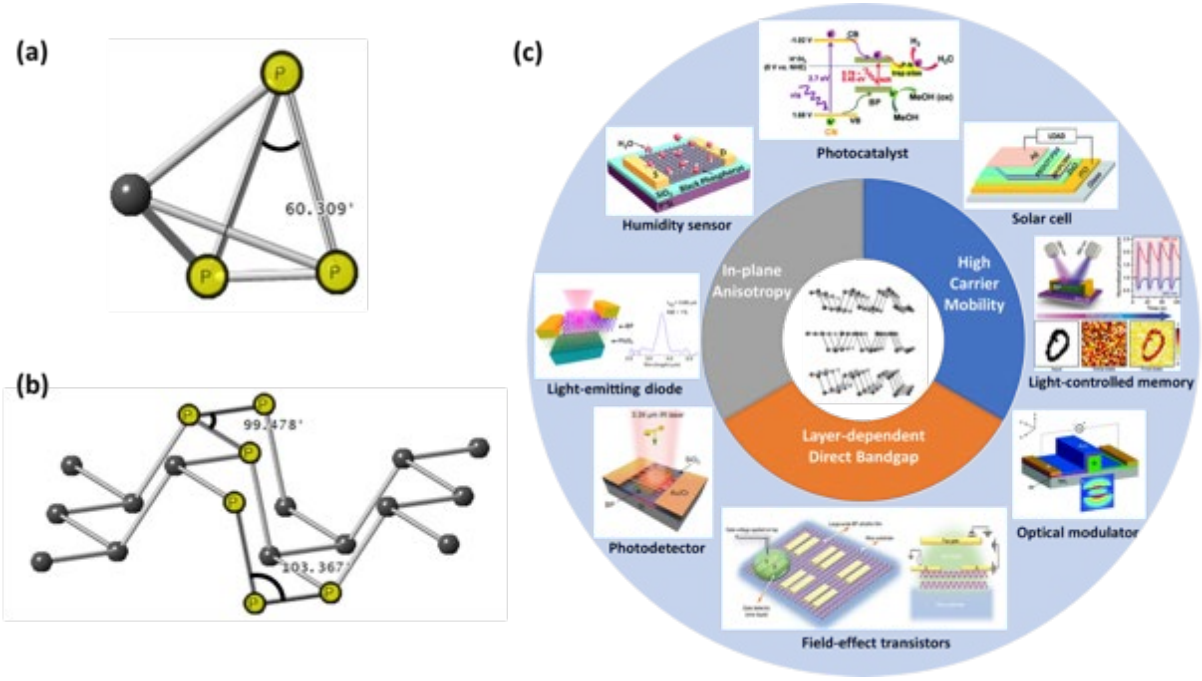

Figure 1 Schematic illustration of (a) Tetrahedron WP P_4 molecule, (b) monolayer phosphorene and (c) Characteristics and applications of low-dimensional BP. (c) Reproduced with permission from Ahmed et al., Adv. Mater. **33**, 2004207 (2021), Copyright 2020 Wiley-VCH GmbH [33], Guo et al., Nano Lett. **16**, 4648 (2016), Copyright 2016 American Chemical Society [34], Miao et al, ACS Appl. Mater. Interfaces. **9**, 10019 (2017), Copyright 2017 American Chemical Society [35], Wu et al., Nat. Mater. **20**, 1203 (2021), Copyright 2021 Springer Nature Limited [36], Bai et al., J. Mater. Chem. A **5**, 8280 (2017), Copyright 2017 Royal Society of Chemistry [37], Lin et al., Nano Lett. **16**, 1683, (2016), Copyright 2016 American Chemical Society [38], Zhu et al., J. Am. Chem. Soc. **139**, 13234 (2017), Copyright 2017 American Chemical Society [39] and Wang et al., Nano Lett. **20**, 3651 (2020), Copyright 2020 American Chemical Society [40]

The unique characteristics of BP originate from its distinct crystal structure. BP shows a direct bandgap feature regardless of layer numbers which distinguishes it from most other 2D semiconducting materials that possess direct bandgap only at certain thicknesses. Hence, BP is a suitable semiconductor for potential developments such as effective photo-electrical conversion and remarkable light-emission devices.[41] Because of the strong electronic state coupling within BP layers, the layer-dependent band gap of its bulk state, single-layer, and few-layer forms are relatively different.[10] The band gap of bulk BP is around 0.3 eV. [42] Theoretical studies indicate that the band gap of monolayer and multilayer BP ranges from 1.51 eV to 2 eV, with the bandgap energy varying significantly depending on the calculation methods utilized.[17,43] Aside from theoretical studies, numerous experimental investigations on the bandgap of BP have also been conducted. Surprisingly, similar to the theoretical works, the results obtained in these works also vary with the methodology employed. The bandgap for monolayer BP is 2.05 eV using the surface-sensitive high-resolution scanning tunneling spectroscopy, which focuses on the topmost layer detects of the BP surface.[44] In comparison, the defects-insensitive absorption spectroscopy indicates that the optical bandgap of monolayer BP is 1.73 eV.[19] The absence of interlayer hybridization near the top of the valence and bottom of the conduction band is expected to induce an increase in the bandgap of single-layer BP.[45] Although the bandgap values obtained through theoretical calculations and experimental results fluctuate in a range, a general trend of decrease in the bandgap with increasing number of layers can always be observed due to the vdW interaction between layers that promotes band splitting.[46]

Another outstanding property that has drawn great research interest to this novel material is its high carrier mobility in comparison to the TMDs family.[47] Alike the thickness dependency of bandgap of TMDs, the mobility of 2D BP is also thickness dependent.[10] At

120 K, the hole mobility of 15 nm-thick BP is 600 $cm^2V^{-1}s^{-1}$ along the light and heavy effective mass directions.[48] For a 10 nm thick BP, the maximum mobility reaches up to 1000 $cm^2V^{-1}s^{-1}$.[10] Monolayer BP is reported to have ultra-high hole mobility in the order of 10000 $cm^2V^{-1}s^{-1}$ as well as abnormal elastic characteristics. [49] Moreover, BP also demonstrates a moderate current on/off ratio ranging from around 10^4 to 10^5.[50,51] At room temperature, 5 nm-thick BP nanosheets were employed in transistors and showed a current on/off ratio of 10^5 with great current saturation property.[52]

On the other hand, BP features puckered structure and gives rise to in-plane anisotropy property, leading to distinctive angle-dependent carrier mobility anisotropy.[48] Previous theoretical research suggests that the mobility of electrons and holes are anisotropic and asymmetric, whereas the holes have higher mobility along both zigzag and armchair directions.[49] In terms of directional anisotropy, the mobilities of electron and hole in the zigzag direction are greater than those in the armchair direction, with the exception of the monolayer where the zigzag direction has a higher electron conductivity but lower hole conductivity. The anisotropic effective masses of electrons and holes are the primary contribution to the anisotropic transport characteristics.[53] The remarkable angle-dependent qualities provide researchers a new level of freedom when it comes to build novel optoelectronic and electric devices that are not achievable with existing 2D materials. However, the preparation of high-quality 2D BP has primarily relied on bottom-up techniques such as mechanical or liquid exfoliation from bulk crystals, which results in thin layers that were only 5-50 μm^2 in size, far too small to meet the demands of practical applications such as integrated circuits. A critical requirement for achieving a breakthrough worldwide technological impact is the monolithic integration of transistors with interconnects and other components, which requires development of synthesis methods beyond exfoliation to prepare BP thin films in

wafer-scale. Hence, we will introduce the following various techniques developed to fabricate 2D BP with higher yield and more controllable shape.

3. Pro-thinning treatment after exfoliation

Ultrathin BP flakes can be prepared via top-down processes, including mechanical and liquid phase exfoliations, however these approaches are lacking reliable thickness control. Therefore, exfoliation is frequently supplemented with further thinning treatments such as thermal sublimation and plasma etching, which will be discussed in detail as follows.

The mechanism of thermal thinning of mechanically exfoliated BP was first reported by Hersam's group and characterized by *in-situ* scanning/transmission electron microscopy.[54] The morphology and spectroscopy results indicate that 2D BP decomposed at around 400 °C in vacuum, in contrast to the sublimation temperature of bulk BP (550 °C). Figure 2a-c present the images of nanoflakes heated at 400 °C for 5 min, 8 min, and 12 min, respectively, demonstrating the thinning treatment accompanied to exfoliation. The *in-situ* sublimation starts with eye-shaped defects propagating along the [001] direction and terminating with a thin, amorphous red phosphorus-like skeleton. Based on previous works, Luo et al. reported a layer-by-layer thermal sublimation of BP with a heating temperature below 600 K, and the illustration of this process is shown in Figure 2d.[55] At 500 and 550 K, the thinning rates of heating BP flakes constantly were 0.18 $nm \cdot min^{-1}$ and 1.15 $nm \cdot min^{-1}$, respectively. Figure 2e and 2f show the Raman intensity ratios as functions of BP thickness at different temperatures (room temperature, 500 and 550 K), which was employed for *in-situ* and contact-free BP thickness measurement and thickness regulation throughout the sublimation process. The uniform and defect-free BP flakes with less than 4-layer thickness and 200 μm^2 large lateral

area were effectively and consistently fabricated on Si wafer and graphene/Si substrate, showing promise for large-scale production of high quality few-layer BP.

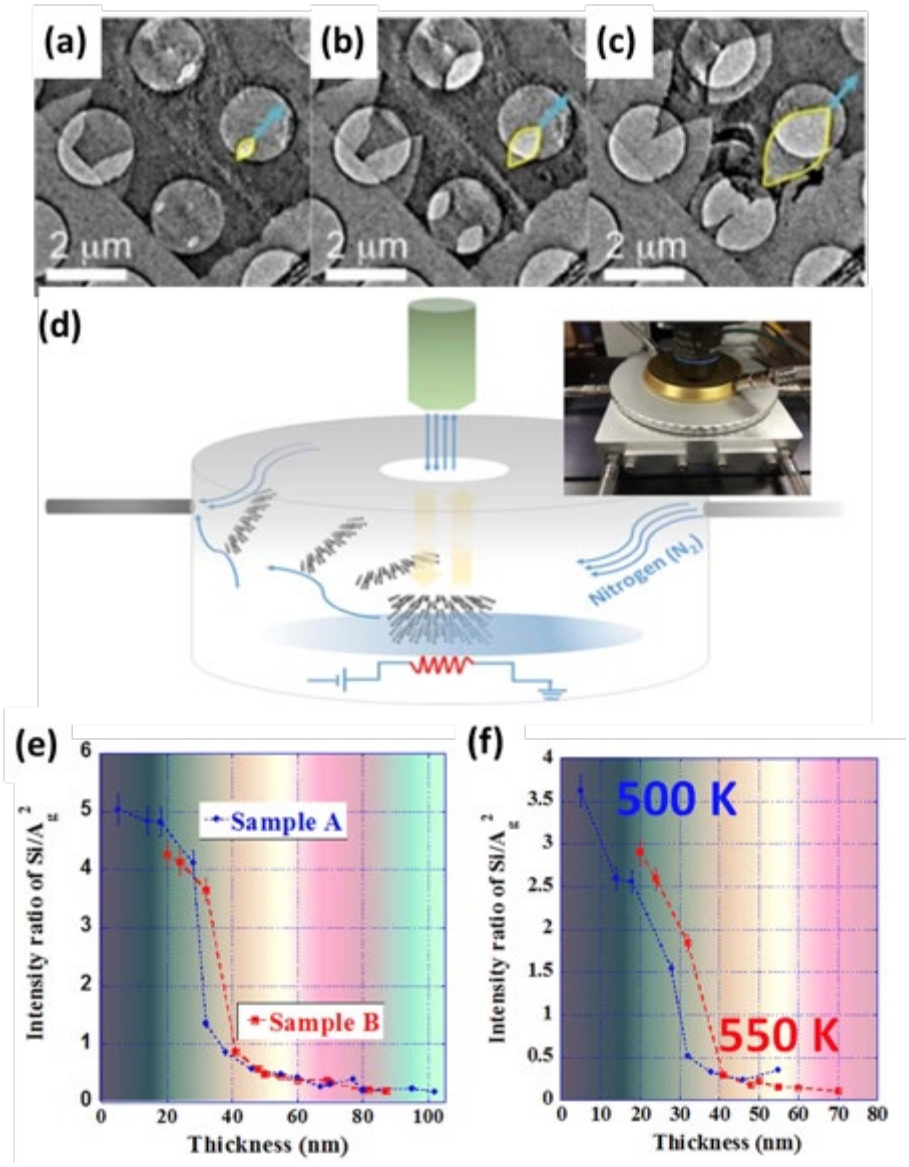

Figure 2 (a-c) Image of eye-shaped cracks (yellow) formation and growth in BP during sublimation. The blue arrow indicates the propagation is alone [001] direction. (d) Schematic diagram of BP sublimation process and the heating stage applied during the thermal sublimation. (e) The Raman intensity ratios of sample A (blue line) and B (red line) verses thickness at room temperature. (f) The Raman intensity ratios of Sample A heated at 500 K and Sample B heated at 550 K Si as a function of thickness. (a) and (b) Reproduced with permission form Liu et al., J. Phys. Chem. Lett. **6**, 773 (2015), Copyright 2015 American

Chemical Society. [54] (c)-(f) Reproduced with permission from Luo et al., Nanotechnology **28**, 285301 (2017), Copyright 2017 IOP Publishing [55]

Meanwhile, instead of sublimating BP flakes directly, Fan et al. introduced a method to oxidize the exfoliated BP in air at 300 °C to 360 °C for 0.5 to 3 minutes to P_2O_5 and then annealed P_2O_5 in the flow of N_2/H_2 mixture gas for 0.5 minute as presented in Figure 3a.[56] Figure 3b shows the atomic force microscope (AFM) image, indicating that the thickness of BP after annealing for 40 seconds in air and 30 seconds in the gas flow of N_2/H_2 at 340 °C is 0.6 nm matching with the thickness of single-layer BP. The orderly-arranged well-preserved atomic structures with no obvious defect of the mechanically exfoliated BP and the flake after annealing for 2 minutes in air and 1 minute in N_2/H_2 mixture at 340 °C are presented in the transmission electron microscopy (TEM) measurement (Figure 3c and 3d). This two-step thermal annealing approach allows an ultra-fast preparation for thickness-controllable BP under moderate temperature processing, which could possibly be utilized in large-scale manufacture. Figure 3e demonstrates the schematic diagram of another straightforward and practical one-step approach for developing an air-stable and thin BP, as investigated by Yang et al. in 2018. [57] This approach starts initially with the oxidation process by heating the thick BP under ambient environment, followed by partial evaporation of the oxidized BP surface through simultaneously heating. Consequently, the BP can be etched with a steady etching rate through modulating the temperature parameters. Thermally generated protective oxide layer is highly stable and thus prevents the degradation of underneath BP layers even contacting with air for 4 days. Moreover, this approach allows the formation of a flat surface and diminishes carrier scattering centers, leading to a considerable improvement in the performance of BP-based field-effect transistor (FET). As shown in Figure 3f, both mobility and on/off current

ratios increase significantly after annealing the samples at 250 °C in ambient condition for 5 minutes (step 1) and another 5 minutes (step 2).

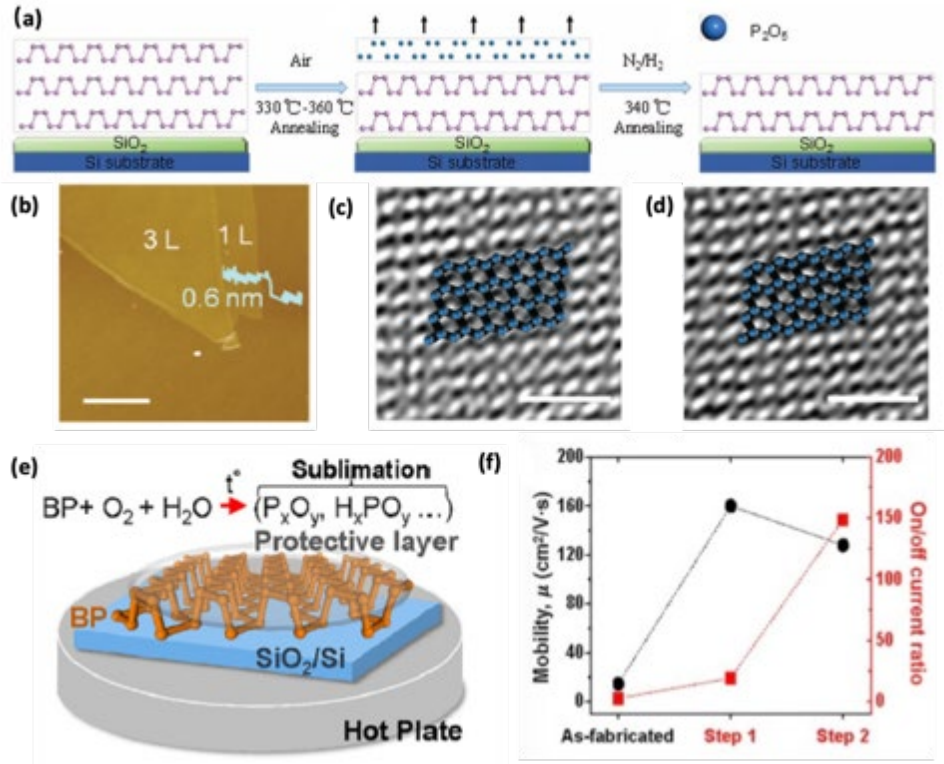

Figure 3 (a) Schematic diagrams of thermal annealing method starting with oxidizing the top layers of exfoliated BP to P_2O_5, followed by sublimation of P_2O_5. (b) The AFM image of BP flake after rapid annealing. High-resolution (HR)-TEM image of the (c) mechanically exfoliated BP and (d) the same flake after thermal annealing. (e) Schematic model of one-step thermal annealing process of thin BP layer production. (f) Field-effect mobility and on/off current ratio under different annealing conditions. (a)-(d) Reproduced with permission from Fan et al., J. Mater. Chem. C **5**, 10638 (2017), Copyright 2017 Royal Society of Chemistry. [56] (e) and (f) Reproduced with permission from Yang et al., Appl. Surf. Sci. 457, 773 (2018), Copyright 2018 Elsevier. [57]

In 2014, the combination of mechanical exfoliation and plasma treatment was developed by Lu et al. as a successful method for producing monolayer phosphorene.[58] After the few-layer BP was mechanically exfoliated from bulk crystal, Ar^+ plasma was applied during the thinning process to produce monolayer phosphorene. Moreover, a viable method was demonstrated to determine the layer number of exfoliated BP flakes relying on the Raman peak intensity in this work. As shown in Figure 4a, the frequency difference between A^2_g and B_{2g} modes of bulk BP crystal is 27.7 cm^{-1} and that of monolayer is 31 cm^{-1}, allowing the Raman shifts to function as an efficient parameter to deduce the thickness of phosphorene. To further overcome the technological obstacles, such as the environmental instability of BP, Jia et al. passivated the FETs built on Ar gas-based plasma-treated BP film with poly(methyl methacrylate) (PMMA) coating to achieve a high field-effect mobility (1150 $cm^2V^{-1}s^{-1}$) and I_{on}/I_{off} ratio (around 10^5) at room temperature as shown in Figure 4b.[59] As presented in Figure 4c, the plasma treatment not only modulates the thickness of the BP flakes, but also removes the degradation of the oxidized BP top layers, leading to an improvement in FET performance and environmental stability.

A mild plasma etching process aiming at reducing the structure degradation was then proposed by Lee et al. [60] As shown in Figure 4d, as the samples were placed in face-down orientation, direct ion bombardment can be avoided. By adjusting the reactive-ion-etching (RIE) conditions used during experiments, the reaction between fluorine and phosphorus permits degradation-free thinning process of BP, while the absence of damage was verified by TEM before and after plasma treatment, as shown in Figure 4e and 4f. Kuriakose et al. have studied the electrical and optoelectronic properties of plasma-treated BP in Ar and oxygen (O_2) atmospheres.[61] They suggested that the O_2 plasma etching method is more beneficial because it allows better thickness control and enhancement in the intrinsic optoelectronic characteristic of BP, owing to the development of an interfacial P_xO_y encapsulation surface, and the

associated defects can contribute to the photoluminescence (PL) emissions at additional wavelengths (presented in Figure 4g), while maintaining the FET electrical performance (shown in Figure 4h). It is also deduced that pristine BP might be used as a functional layer in UV sensors due to its potential to respond to UV irradiation.

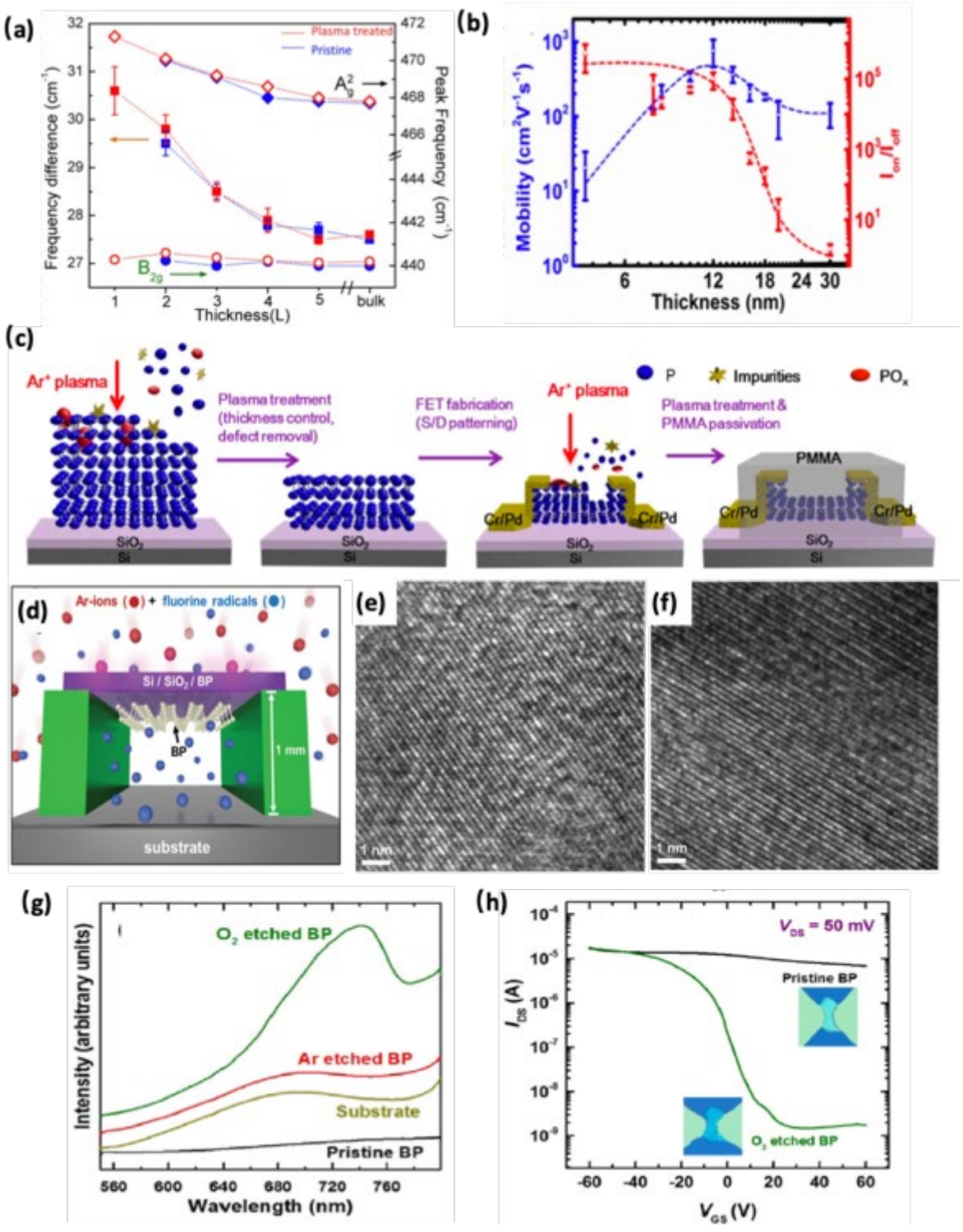

Figure 4 (a) Number of layer dependence of peak frequency of Raman peak A_{2g} and B_{2g} and frequency difference between them. (b) BP film thickness dependence of field-effect mobility and I_{on}/I_{off} ratio. (c) Schematic illustration of the plasma treatment process of BP flake. (d) Schematic diagram of the chemical etching process inside the reactive-ion-etching system chamber. TEM result of BP (e) before and (f) after plasma treatment. (g) Comparison of photoluminescence spectra of pristine and plasma-treated BP flakes. (h) I-V curves of pristine and O_2-etched BP FETs with 50 mV V_{ds} bias. (a) Reproduced with permission from Jia et al., ACS Nano **9**, 8729 (2015), Copyright 2017 Springer Nature. [59] (b) and (c) Reproduced with permission from Lee et al., Mater. Chem. C **4**, 6234 (2016), Copyright 2015 American Chemical Society. [60] (d)-(f) Reproduced with permission from Kuriakose et al., Appl. Mater. Today **12**, 244 (2018), Copyright 2018 Royal Society of Chemistry. [61] (g) and (h) Reproduced with permission from Akhtar et al., npj 2D Mater. Appl. **1**, 1 (2017), Copyright 2018 Elsevier. [62]

Kim et al. have demonstrated a UV/ozone treatment which is a convenient and reliable approach for adjusting the thickness of BP flakes by etching them layer by layer. [63] Compared to plasma treatment, UV irradiation can be generated by a simple and inexpensive equipment, such as a UV lamp. Without changing the position of the BP sample, UV and Raman measurements were applied and the spectra could be captured by positioning the UV source (Hg lamp) within the chamber attached to the micro-Raman system displayed in Figure 5a. As shown in Figure 5b, the full width at half maximum (FWHM) of the BP-related peaks develop a downtrend with increasing duration of UV exposure, while the Si peak remains unchanged. The narrowing BP Raman peaks observed can be linked to the elimination of degraded BP top layers during the UV treatment thinning process. Furthermore, Figure 5c illustrates that the field-effect mobility and on/off ratio of BP-based FETs are enhanced by 48%

and 6800%, respectively. The exploration and application of ultra-thin BP are restricted by its instability in ambient air. The method developed in this work provides a dependable way starting with thick BP flakes, aiming to improve electrical performance of mono- and few-layer BP-based electronic devices. In 2016, a simple and effective chemical etching method mainly using ozone as one of the UV-activated oxygen (UVO) species was employed by Kwon and coworkers.[64] By adjusting the exposure duration under UV light (wavelength shorter than 250 nm) in an oxygen atmosphere, etching of BP nanoflakes down to a sub-nanometer thick thin film is realized. The etching process consists of ozone induced by photolysis of oxygen to oxidize BP into phosphorus oxide, followed by removing the interface oxide through dissolution in phosphoric acid. These procedures are repeated until the desired thickness is achieved. After washing with deionized (DI) water, very flat BP films of predetermined thickness with protective surface oxygen functional group that exhibits improved stability under ambient environment are obtained. The 2D AFM images of the BP flake of each step during the etching process, including right after exfoliation, water rinse, 6 hours and 24 hours exposures in air are illustrated in Figure 5d, respectively.

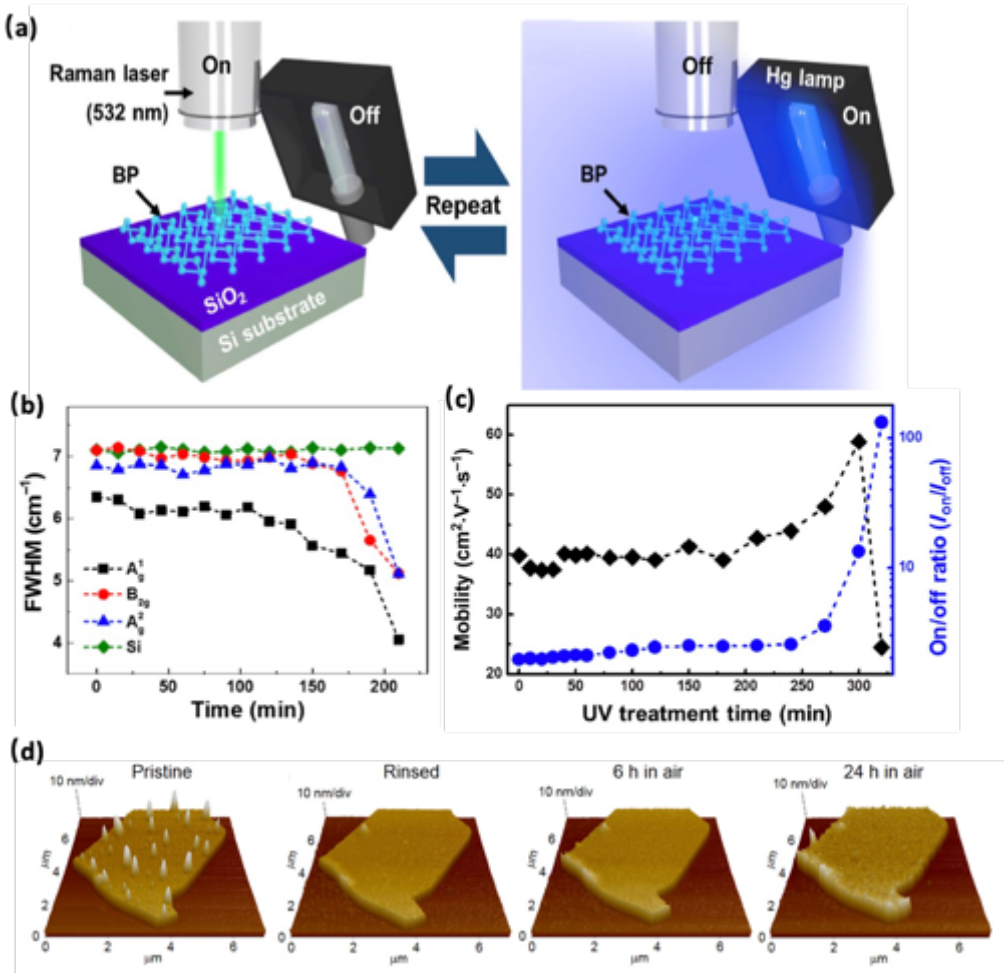

Figure 5 (a) Schematic illustration of experimental setup for Raman spectra collection with UV/ozone treatment. (b) Time dependence of FWHM of A^1_g, B_{2g}, and A^2_g mode. (c) Variation of field-effect hole mobility and on/off ratio of BP FET with the UV treatment time. (d) 3D AFM height images of a BP flake under different conditions. (a)-(c) Reproduced with permission from Kim et al., Nano Res. **9**, 3056 (2016), Copyright Springer Nature. [63] (d) Reproduced with permission from Kwon et al., ACS Nano **10**, 8723–8731 (2016), Copyright American Chemical Society. [64]

Laser thinning approach of BP is also one of the widely investigated methods which is capable of controlling the thickness of exfoliated BP. In 2015, Lu et al. have proposed a simple and reliable laser pruning method for reducing the number of layers in ambient environment.[65] Phosphorene oxides and sub-oxides are generated during the thinning

process. By adjusting the laser power, the degree of oxidation can be regulated. The contrast of reflection color of the BP flake under optical microscope before and after the laser pruning process can be observed in Figure 6a. In addition, AFM results displayed in Figure 6b and 6c further confirm that the thickness of the laser pruned region is reduced by around 11 nm. This simple approach can accomplish localized band gap engineering of the BP thin films as the band gaps of the sub-oxides are reliant on the concentration of oxygen applied. Figure 6d shows the micro-patterns created on the sub-oxide flakes with distinct optical and fluorescent characteristics. The rough edges of BP are not observable under fluorescence microscopy, leaving the polychrome micro-patterns visible only, with different colors that easily altered by adjusting the excitation wavelength. Instead of turning pristine BP flakes into phosphorus oxide layer, Kundu et al. have proposed a one-step technique for precise patterning on few-layer BP utilizing low-power 532 nm laser treatment for producing metal-free surface-enhanced Raman spectroscopy (SERS) substrates.[66] The thickness of BP flakes can be evenly reduced from 200 nm to 4 nm (2 to 3 layers) with great accuracy under the application of an optimum laser power and exposure duration, as demonstrated in Figure 6e. Figure 6f shows the Raman spectra for 12 different thicknesses from 147 nm to 4.5 nm through the low power focused laser thinning treatment. The positions of the Raman peaks remained unchanged, indicating that the pristine quality of BP was preserved properly during the laser thinning process. In comparison with mechanically exfoliated BP nanoflakes, the pro-thinning procedures not only increase the yield during the fabrication process, but also enable the synthesis of 2D BP with controllable thickness and size.

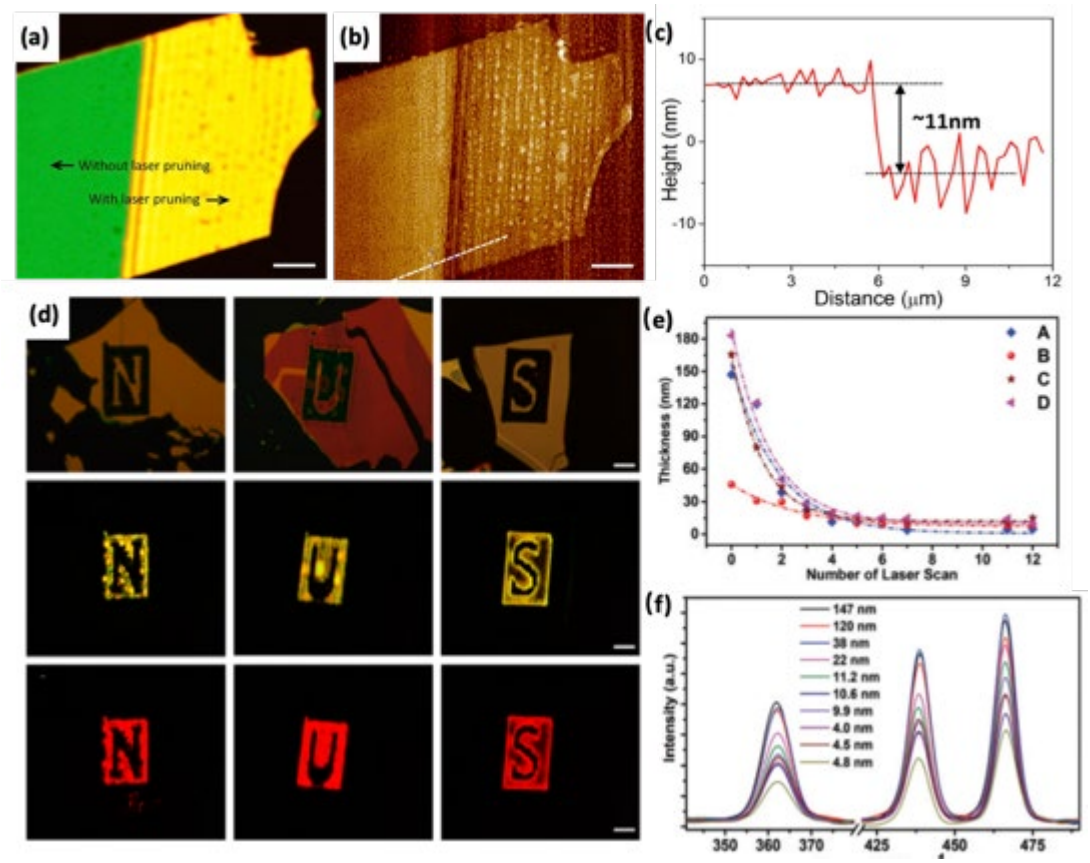

Figure 6 (a) Optical image and (b) AFM topography of a BP flake after laser pruning. (b) AFM profile. (c) Height profile across the with and without laser pruning areas. Scale bar: 5 μm. (d) Optical image, FM images of excited by blue light (460-490 nm) and green light (510-550 nm). Scale bar: 10 μm. (e) Thickness of BP flakes as a function of number of laser scan. (f) Raman spectra of BP thickness reducing from 147 nm to 4.5 nm during the laser thinning process. (a)-(d) Reproduced with permission from Lu et al., ACS Nano **9**, 10411 (2015), Copyright 2015 American Chemical Society. [65] (e) and (f) Reproduced with permission from Kundu et al., Nanoscale **11**, 16245 (2019), Copyright 2019 Royal Society of Chemistry. [66]

4. Conversion from red phosphorus to BP

Owing to the rigorous growth requirements and poor yield of BP, attempts have been focusing on converting red phosphorus (RP) to BP under high temperature and hydrostatic pressure

conditions since 1937.[67] Before synthesizing few-layer BP, BP single crystal growth from RP with Sn/SnI_4 as mineralization additives has been achieved by Köpf and this approach brought with two advantages, namely reducing the amount of side phases drastically and shortening the reaction time.[68]

As much research in recent years are focused on 2D materials, a technique for large-area (with diameter around 4 mm) BP thin film production on flexible substrates has been presented. [69] As plotted in Figure 7a and 7b, a RP thin film was initially formed on flexible substrates by thermal deposition. Then, the RP thin film was pressurized in an anvil cell with application of a pressure greater than 8 GPa at room temperature to convert to a BP film. The rise of absorption near 2200 cm^{-1} can be observed from Figure 7c, suggesting that the bandgap of BP thin film is around 0.28 eV which is similar to the one reported in exfoliated nanoflakes. In 2017, a moderate approach was reported for synthesizing BP nanosheets from RP microspheres by employing NH_4F to lower the activation energy of RP based on phosphorus phase change and Gibbs free energy theory.[70] The photocatalytic hydrogen formation from water performance of this kind of layered BP is extremely efficient. Furthermore, BP is one type of considerable anode materials for lithium-ion batteries exhibiting high electrochemical functionality. Inspiringly, highly crystalline BP thin films were fabricated on a 5 mm sapphire substrate, accomplished by RP thin film deposition and RP to BP conversion at 700 °C and 1.5 GPa (Figure 7d).[71] Continuous multi-crystalline BP thin film with the thickness around 50 nm can be observed in Figure 7e, while the inset AFM image illustrates that the height of ripples is about 40 nm. Figure 7f further indicates that the boundary between two adjacent domains has diverse ripple orientations. The FET constructed with the synthesized BP thin film showed a field-effect mobility of about 160 and 200 $cm^2V^{-1}s^{-1}$ at room temperature and 90 K, respectively. In addition, Figure 7g presents the formation of a perfect hBN/BP heterojunction, where the hBN layer was coated onto RP before conversion.

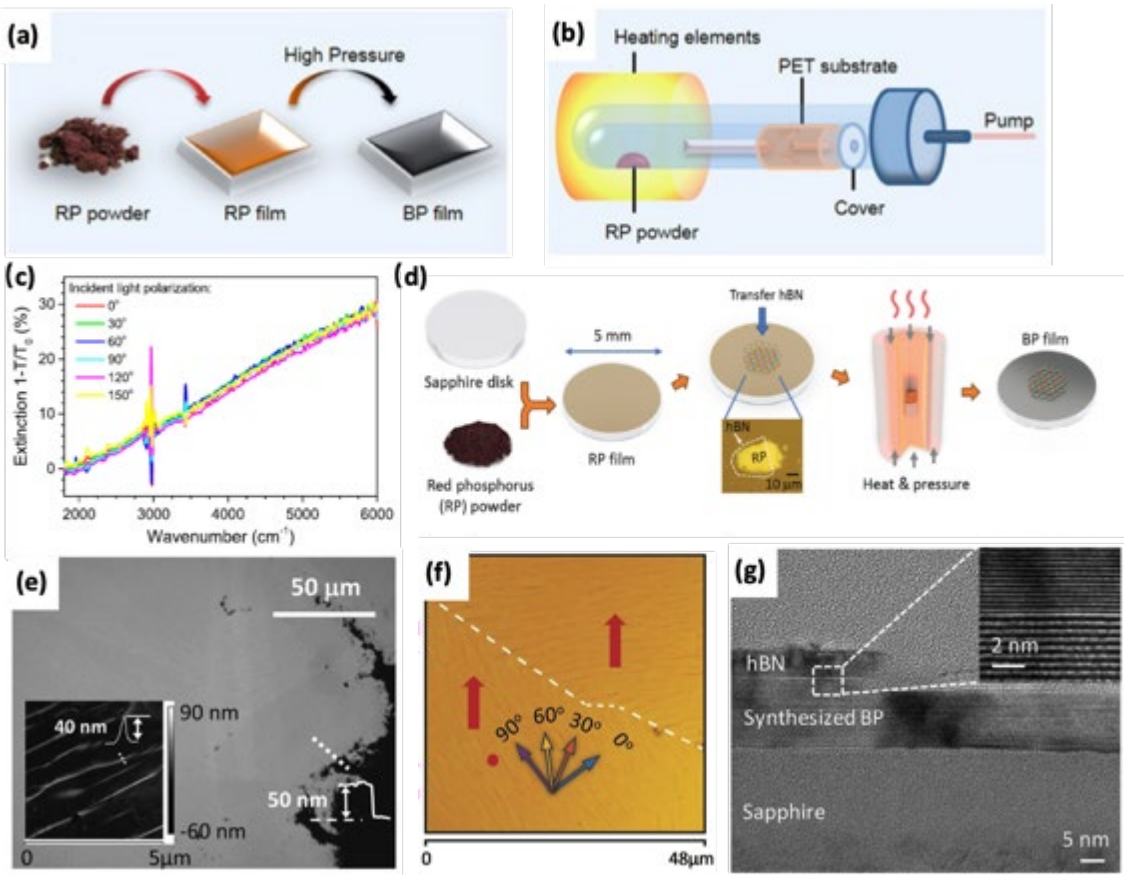

Figure 7 (a) Strategy and (b) Schematic apparatus illustration for the fabrication of large-area BP thin film on a flexible substrate. (c) Optical extinction of BP thin film with various incident light polarization. (d) Synthesis process of BP thin film on sapphire. (e) Optical image of synthesised BP with visible ripples. Inset: AFM image of ripples. (f) Optical image of boundary of two domains. (g) Cross-section TEM image of h-BN/BP interface. (a)-(c) Reproduced with permission from Li et al., 2D Mater. **2**, 31002, (2015), Copyright 2015 IOP Publishing. [69] (d)-(g) Reproduced with permission from Li et al., Adv. Mater. **30**, 1703748 (2018), Copyright 2018 Wiley-VCH Verlag GmbH. [71]

In order to search for mild synthesis conditions, Izquierdo et al. directly grow BP onto silicon and silicon dioxide substrate under a pressure smaller than 1.5 MPa and temperature of 650 °C proceeded with red phosphorus, Sn and SnI_4 via seeding vertical growth process.[72] A uniform crystal surface of the BP microbelt can be visualized in Figure 8a. A considerable

concentration of crystalline SnI_x inclusion can be observed as bright spots from the cross-sectional TEM image (Figure 8b). As shown in Figure 8c, no oxidation/degradation bubble is observable from the BP surface under air exposure for 170 days. During the fabrication process, an *in-situ* passivation layer of Sn can protect the BP layer and reduce the detectable phosphorus oxidation rate, in this way the BP layer can be placed stably in ambient environment for almost four months. Apart from silicon or silicon dioxide, other substrates are also suitable for BP fabrication. Han et al. directly synthesized highly crystalline thin-film BP onto GaN (001) substrate.[73] The interface between GaN and BP was quite sharp and the formed heterojunction interface is shown in Figure 8d and 8e. Density functional theory (DFT) calculations were utilized to investigate the detailed atomistic processes involved in the P adsorption on GaN (001) surface, because there are no nitrogen atoms directly below the vacancy formed by three adjacent gallium atoms, the P adatoms have lowest adsorption energy of on the GaN (001) surface. According to the results obtained through the self-consistent geometric optimization, the a-axis of GaN and BP is quite close, while the b-axis is not. As GaN and BP possess hexagonal and orthorhombic structures, respectively, rotating GaN by 30° resulting in a smaller mismatch. As shown in Figure 8f, the mismatch degree of the GaN/BP heterostructure along b axis is 4.4%, indicating coherent growth of BP in nature. Figure 8g further illustrates the kinetic strategy for synthesizing BP via epitaxial growth on GaN. Owing to the relatively weak P-P bond compared to the adsorption energy of an isolated P adatom on the GaN (001) surface, it is confirmed that the P adatoms tend to stay separated rather than forming clusters. The P adatoms gradually cover the GaN surface and form layered structure instead of single P adatom arrangement due to the small lattice mismatch of GaN/BP heterostructure.

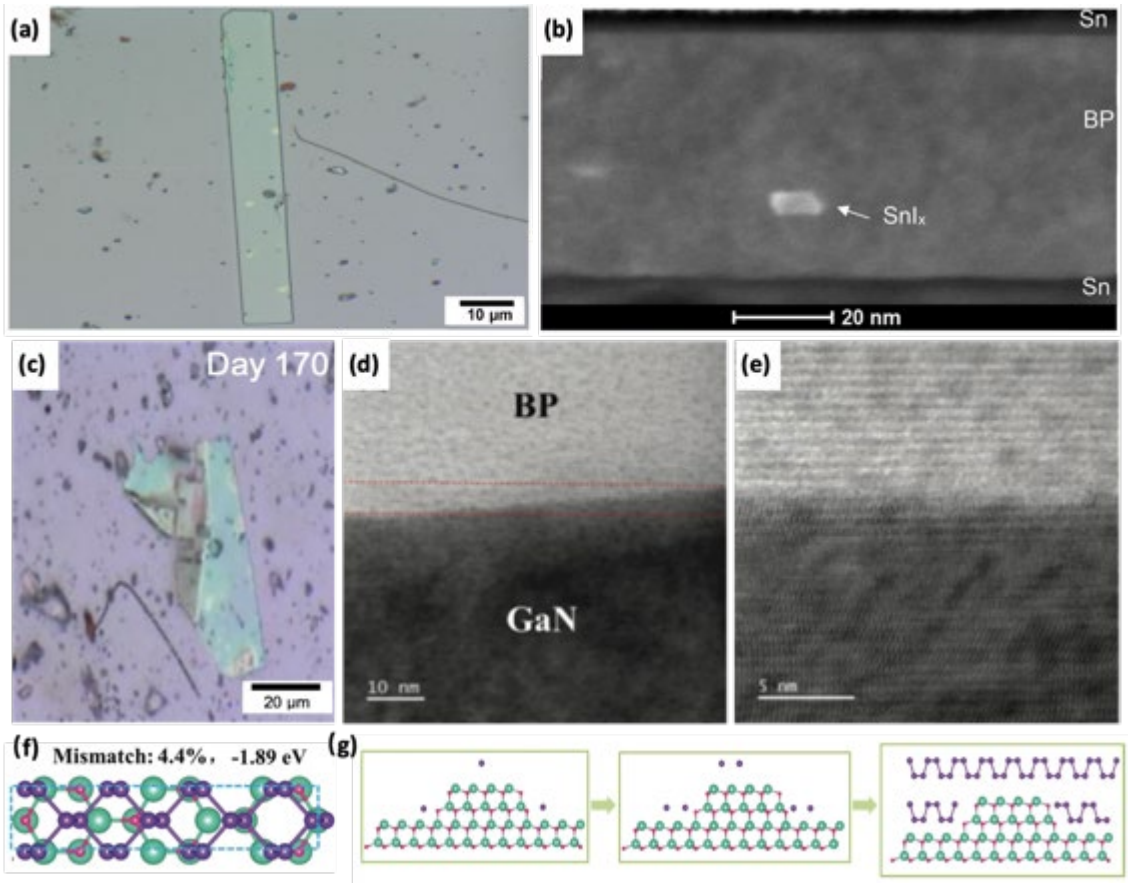

Figure 8 (a) Optical image of BP microbelt. (b) Cross-sectional TEM image of the Sn/BP/Sn heterojunction. (c) Optical image of BP flake at day 170. (d) Cross-section STEM and (e) enlarged image of GaN/BP interface. (f) Top view of the lattice mismatch and absorption energy based on the heterojunction model constructed with a $1 \times 3\sqrt{3} \times 1$ GaN supercells and a $1 \times 4 \times 1$ BP supercells. (g) Schematic illustration of the thin-film BP fabrication process via epitaxial growth on GaN (001) surface. (a)-(c) Reproduced with permission form Izquierdo et al., ACS Nano **13**, 7091 (2019), Copyright 2019 American Chemical Society. [72] (d)-(g) Reproduced with permission from Han et al., Nanoscale **12**, 24429 (2020), Copyright 2020 Royal Society of Chemistry. [73]

5. Direct large-area synthesis methods for 2D BP

Although 2D BP can be prepared through the traditional techniques described in previous sections, these methods still exhibit various limitations. For instance, the dimensions of BP nanoflakes prepared through pro-thinning treatment after exfoliation are usually small, and these methods exhibit restricted scalability. For converting RP to BP, the efficiency during the conversion process is relatively low, as RP vapor can transform into WP or remain RP adhering to the tube's surface. The possible involvement of WP raises a potential issue of safety, owing to its poisonous, highly reactive and inflammable characteristics. Furthermore, the high-pressure and high-temperature equipment mentioned in previous works is hard to equip in most of research labs and places of manufacture. What's worse, the high-pressure approach is risky and unable to maintain sustaining production. Therefore, most of the approaches as above-discussed are time-consuming, high cost, and only can be applied in a small scale.

Large-area fabrication for numerous 2D materials has recently become a central issue beneficial for both fundamental research and emerging applications, particularly introduced in the research prospects of previous review papers.[74-77] For future BP commercialization, it is imperative to explore facile and mature techniques for large-area phosphorene generation under readily controlled circumstances. Therefore, the synthesis process requires a better understanding at the fundamental level for mass production of 2D BP. In this section, we will retrospect the large-scale fabrication methods for BP, including chemical vapor deposition (CVD), pulsed laser deposition (PLD) and so on. These methods listed above are often classified as "bottom-up" approach, which are all part of the synthesis methods with inherent properties that makes large-scale materials processing possible.

5.1 Chemical vapor deposition

CVD is widely recognized as one of the most prevalent methods for fabricating 2D materials which offers tantalizing opportunities for the synthesis of large-area, uniform, and high-quality 2D thin films including graphene and TMDs.[78-80] The BP prepared through top-down methods is not sufficient to apply in large-area electronic devices, while BP films with optimal lateral size and controllable thickness can be achieved simultaneously by applying the gas-assisted strategy.

In recent year, Zhang and co-workers designed a novel strategy for high-crystalline large-sized BP films epitaxially fabricated on silicon substrate where Au_3SnP_7 acts as the seed nucleation (see Figure 9a).[81] The lattice spacing of the Au_3SnP_7 is similar to the lattice parameters of BP, which can avoid atomic lattice mismatch. Moreover, the thickness and lateral dimensions of the BP films can be adjusted by the temperature gradient between the source at low temperature side and substrate at high temperature side, and the BP films with well-controlled thickness from 10 to 200 nm are shown in Figure 9b. Figure 9c displays the cross section of an atomic layer from the as-grown BP film, presenting a distinct layered structure with 0.5 nm spacing, in consistence with the features of crystalline BP. The HRTEM image in Figure 9d further depicts the atomic structure of the crystalline BP film, while no obvious impurities or defects can be observed, indicating the distinct phosphorus atoms devoid of apparent impurities or defects and a uniform symmetric orthogonal crystal structure. The back-gate FETs based on the as-grown BP thin films (thickness around 8 nm is adopted) to investigate the electrical characteristics of synthesized BP films. Noticeably, the FETs show a p-type ambipolar feature with the mobility over 1000 $cm^2V^{-1}s^{-2}$ at room temperature and a high current on-off ratio of 10^6 as displayed in Figure 9e. These results reveal that the electrical performance of the as-grown BP films is comparable to those observed from BP nanoflakes exfoliated from bulk crystal. Besides, the lamellar structure BP films shows a more significant PL intensity compared with the densely-squeezed layered BP as shown in Figure 9f, because

the nano-gaps distributed in BP atomic layers decrease the charge transfer and lead to a more efficient confinement of the electron-hole pairs. Such electron-hole recombination enhancement in turn increases the photoluminescence responses.

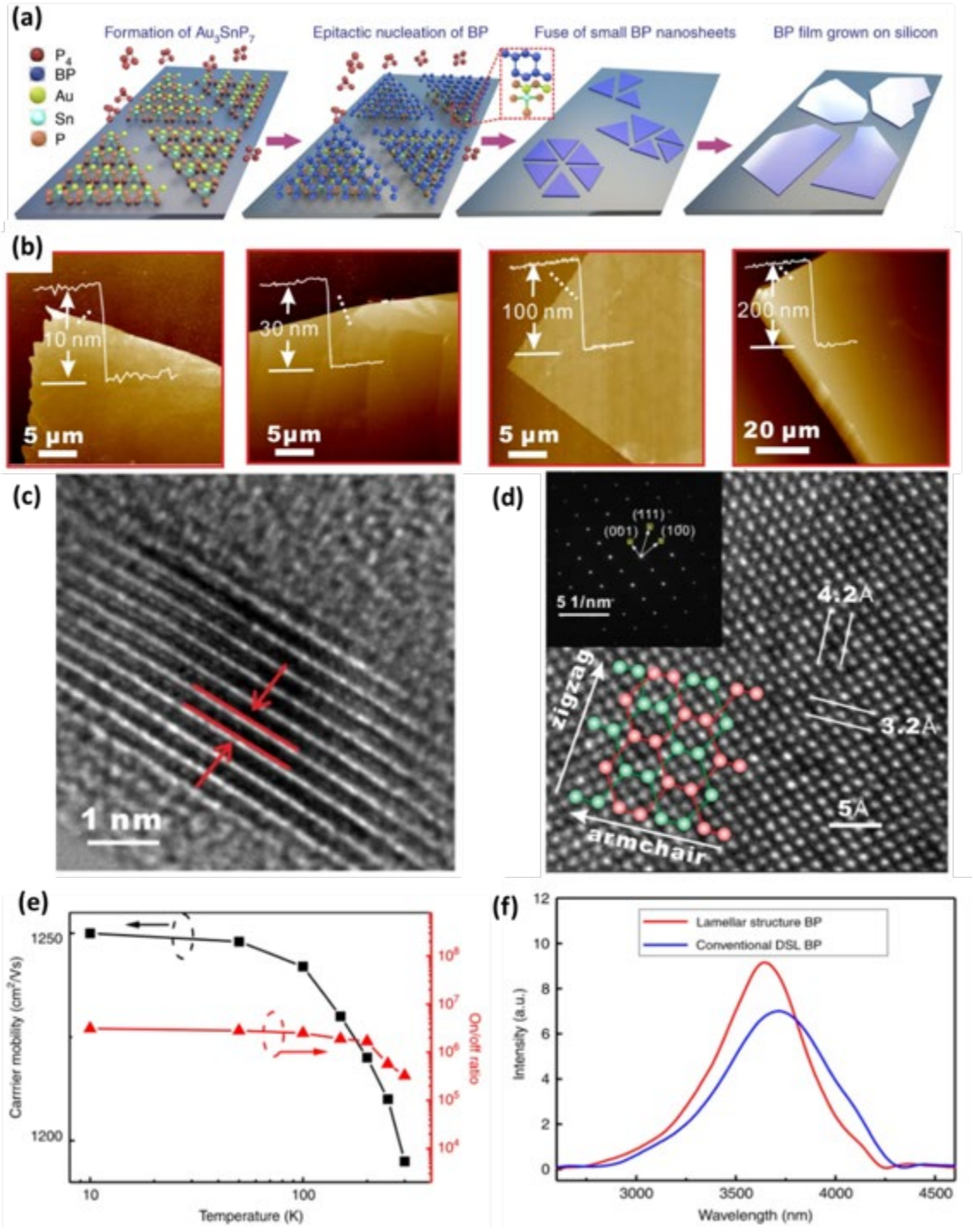

Figure 9 (a) Schematic diagram of the growth process of BP crystalline films on silicon substrate. (b) AFM images of the BP films with thicknesses from several to hundreds of nanometers. (c) A cross-sectional BP atomic layer imaged by HRTEM. (d) Output and transfer characteristics of the FETs based on the synthesized BP film. (e) The temperature dependence of carrier mobility and current on/off ratio in a synthesized BP film. (f) PL spectra of BP with the as-grown lamellar structure and derived from bulk crystal. Reproduced with permission from Xu et al., Nat. Commun. **11**, 1, (2020), Copyright 2020 Springer Nature. [81]

5.2 Pulsed laser deposition

Up to now, CVD is a main method for depositing wafer-scale 2D materials. Our group's research results imply that PLD may offer an important alternative to CVD for 2D material growth. particularly when CVD has proven to be difficult or unsuccessful to make some specific ultrathin films.[82][83][84] In 2015, we fabricated wafer-scale uniform amorphous BP ultrathin films with 53 nm thickness as shown in Figure 10a.[85] The experimental results further suggest that the band gap of amorphous BP sample decreased gradually from 0.8 eV to 0.21-0.26 eV when thickness increased from 2 to 8 nm, consistent to the previously reported layer dependency in bandgap energy of 2D BP nanoflakes.[86] In contrast to other fabrication approaches demanding for extreme fabrication condition such as a high growth temperature, large-area BP thin films can be synthesised at a much lower temperature of 150°C via PLD approach. In addition, FETs based on amorphous BP (a-BP) films of various thicknesses have been fabricated. Figure 10b presents the p-type behaviour of the 2-nm-thick BP based FET, where Figure 10c illustrates the mobility and on/off ratio of this device to be 14 $cm^2V^{-1}s^{-1}$ and 10^2, respectively. Also, the field-effect mobility is steadily improved as the thickness of the a-BP ultrathin films is increased from 2 to 10 nm, while the on/off ratio decreases. Although the

performance of amorphous BP films was relatively poor, the PLD grown sample is superior in some aspects to other amorphous materials.[87] Very recently, great advances in the fabrication of crystalline BP thin films are achieved by a controlled PLD strategy. Our team has demonstrated a unique and controllable PLD technique for synthesizing high-crystallinity centimetre-scale BP thin film, which is published in *Nat. Mater.* (2021) [49]. In the PLD process, the laser ablation creates a plasma-activated area that is desireable for the formation and transportation of BP cluster under energetic high-temperature and high-pressure conditions during the growth process (Figure 10d).[36] With precise control of laser pulse and temperature of substrate, unidirectional growth and cluster merging of remarkable homogeneity BP thin films with well-defined layered number have been promoted, as shown in Figure 10e. To gain an insight into the BP growth by PLD, theoretical simulations of the laser-activated behaviour of surface BP layers are performed in our study. It indicates that the BP clusters are likely to form within the high-pressure region created by the controlled low-fluence pulsed laser, which subsequently facilitate the growth of the BP film on the substrate. Moreover, FET arrays based on the as-grown BP were then fabricated with ionic liquid applied as a gate dielectric to further study the electrical characteristics (see Figure 10f). Figure. 10g and 10h show that the BP ultrathin film-based FETs not only have a typical p-type transferring behaviour, but also exhibit high thickness-dependent carrier mobility reaching up to 213 $cm^2V^{-1}s^{-1}$ and 617 $cm^2V^{-1}s^{-1}$ at 295 and 250 K, respectively. Moreover, as depicted in Figure 10i, the PLD-grown crystalline BP films present remarkably uniform electrical properties at centimetre scale, differing from the most reported BP nanoflakes with restricted lateral size demonstrated. More importantly, the technique of PLD shows intriguing features facilitating device fabrication, including well-controllable thickness, stoichiometric growth, rapid growth and high compatibility with the production of multi-layered heterostructures, simply by rotating multiple targets without breaking the vacuum.[88,89] Therefore, PLD is expected to play an important role in large-

area and high-quality BP thin film fabrication, which is promising to combine with nanofabrication technique for practical device applications.

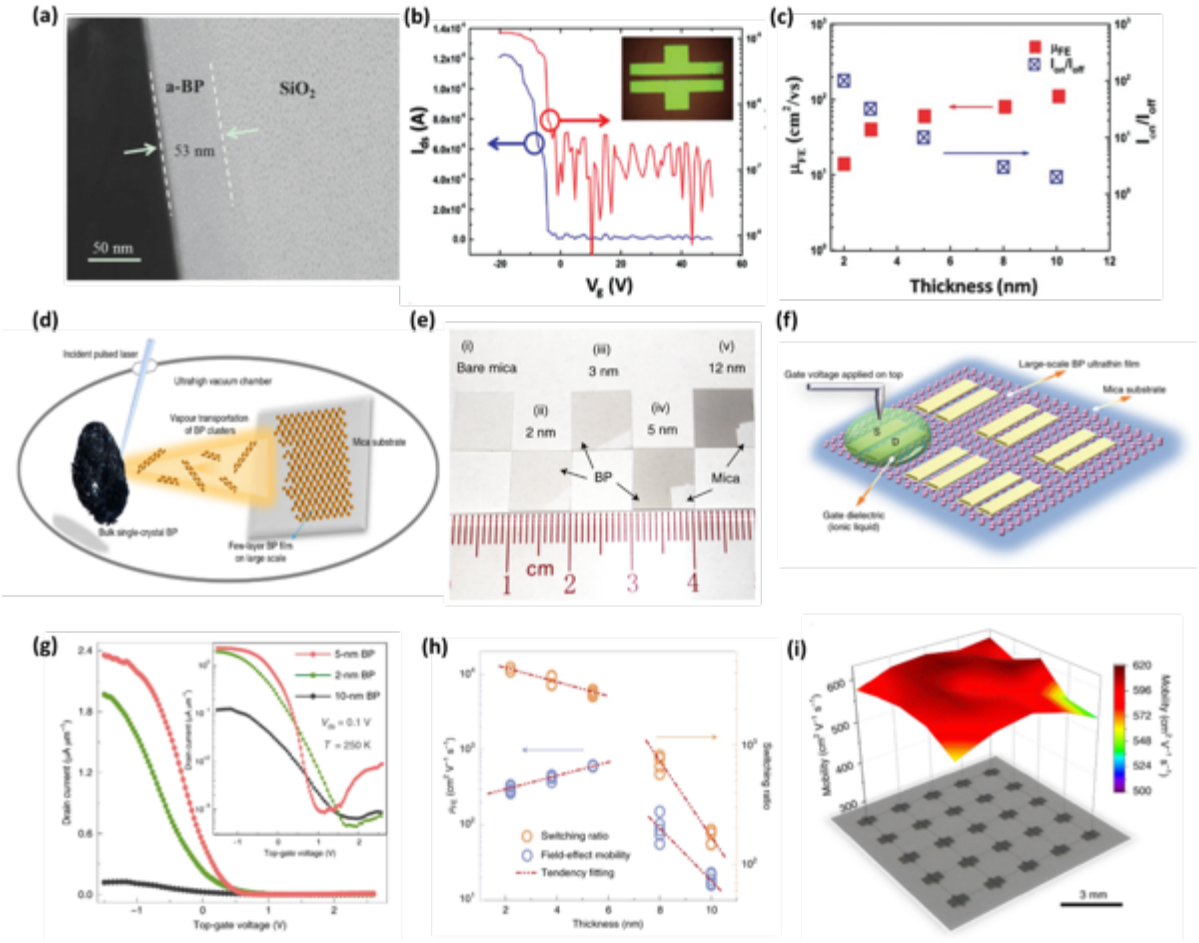

Figure 10 (a) Cross-sectional TEM image of PLD-prepared wafer-scale amorphous BP. (b) The transfer characteristic of the FET based on ultrathin BP film with thickness of 2 nm at V_{ds}= 1 V. (c) The thickness dependence of field-effect mobility and on/off ratio of the FET as a function of the thickness of a-BP films. (d) Schematic diagram of the fabrication of few-layer BP films through controlled PLD process. (e) Optical images of (i) bare mica and as-deposited centimeter-scale BP films with thickness of (ii) 2 nm, (iii) 3 nm, (iv) 5 nm, and (v) 12 nm. (f) Schematic illustration of top-gated BP FET arrays. (g) Transfer curves of FETs based on as-grown BP films with different thicknesses in linear and logarithmic (inset) scale at 250 K. (h) The field effect mobility (μ_{FE}) and switching ratio of the FETs as a function of BP thickness.

(i) Three-dimensional carrier mobility color map derived from 25 FETs based on BP film with 5 nm thickness at 250K. (a)-(c) Reproduced with permission from Yang et al., Adv. Mater. **27**, 3748 (2015), Copyright Wiley-VCH Verlag GmbH. [85] (d)-(i) Reproduced with permission fromWu et al., Nat. Mater. **20**, 1203 (2021), Copyright 2021 Springer Nature Limited [36]

Table.1 Comparison of 2D BP nanoflakes/thin film prepared through different fabrication methods.

Manufacture method	Thickness (nm)	Lateral dimension (μm)	On/off ratio	Hole mobility ($cm^2 V^{-1} s^{-1}$)	Reference
Mechanical Exfoliation	5-10	~ 5	10^5	~ 1000	[10]
Mechanical Exfoliation	5	/	10^4	286	[45]
Liquid-Phase Exfoliation	5-20	Few	10^3	0.58	[90]
Solvent Exfoliation	16-128	Several	10^4	50	[91]
Rapid thermal thinning	0.6	Several	10^5	337	[56]
Ar^+ plasma thinning	2-10	Several	10^5	1150	[59]
Ion bombardment-	20	<10	~ 10	~ 70	[60]

Free plasma etching					
Ozone treatment	~ 5	~ 40	132	59	[63]
RP to BP conversion	50	4000	200	0.5	[69]
Epitaxial nucleation and lateral growth	5-10	Hundreds	10^6	1400	[81]
Pulsed laser deposition	1.1-12	10^3	/	213 (295K) 295 (250K)	[36]

6. Conclusion and future perspectives

In summary, BP has drawn huge attention as a p-type 2D semiconductor with great potential because of its promising electrical and photonic properties. Particularly, in comparison with other 2D materials (e.g., graphene, TMDs, and so on), 2D BP is proved to be a promising 2D semiconductor with moderate bandgap that is thickness dependent and suitable for broad range of light absorption and desirable current-switching abilities. Moreover, BP exhibits relatively high carrier-mobility of both electrons and holes, simultaneously fulfilling the requirements of high-performance nano-electronic applications with bipolar characteristics.[92] Nevertheless, further research and wider potential application of BP are highly dependent on the development of preparation and compatible integration technologies. The manufacturing technique, exfoliation process, and surface treatment are increasingly crucial for the performance of the ultrathin 2D BP used in electronics and photonics. Table 1

summarizes and compares the 2D BP nanoflakes/thin film prepared through different fabrication methods and their electrical performance. In contrast to the time-consuming method of preparing a single device from one exfoliated BP nanoflake, FET arrays can be easily fabricated to evaluate the electrical performance of the PLD grown BP. [36] More importantly, the performances of those devices prepared by the methods beyond exfoliation are comparable to those of exfoliated ones with similar thickness, which may facilitate mass production while efficient material preparation methods can greatly expand their practical uses and industrial applications. This review starts with the fundamental structure and intrinsic characteristics of BP, demonstrating a broad outlook of the original motivation for extensive scientific interest in BP. Next, the exfoliation followed by thinning treatment, conversion from RP to BP, and large-area synthesis approaches (CVD and PLD) are discussed, depicting the challenge of scaling down the thickness of the BP.

As BP is held together by a weak vdW interlayer interaction, it can be easily exfoliated to obtain single or multiple layers of BP nanosheets, which is the simplest method to prepare 2D BP with few defects but at low yields. Pro-thinning treatments are employed after exfoliation to improve the yields, whereas the size of products (e.g. thickness and dimension) can be adjusted. However, few researchers have addressed the problems, such as plasma bombardment damage; non-uniform treatment of reactive oxygen species and UV light; the possibility of amorphous and phase transition within thermal process and laser pruning. Regarding surface treatment approaches, the electrical state of the BP surface and the heterojunction interface, as well as their influence on carrier transport of the treated BP thin films and heterostructures, need further investigation. In-depth understanding of these properties will beneficial for the BP's potential application in novel devices and systems.

In comparison to top-down methods with auxiliary post-processing procedures, the common objective for investigating numerous vdW layered materials that will be used in the

future integrated electronics industry is to design wafer-scale bottom-up growing methods for high-quality 2D films. Existing well-developed approaches for the wafer-scale growth of typical 2D materials might provide valuable experiences for growing other 2D materials.. In comparison with graphene or TMDs, the uniform and wafer-scale growth of BP appears to be a barrier in the manufacture and assembly of different BP-based electrical, photonic, mechanical devices, and its immense potential for use in current semiconductor applications (e.g. integrated circuits). BP has just recently entered the stage of large-area development, with only a few research works demonstrating the large-scale BP film growth through a bottom-up approach, which has great significance for further research and application development of BP. Further studies based on these wafer-scale samples, such as design and fabrication of large-scale integrated circuits, large-area surface treatment and protection; combination, and application design with other large-scale 2D-material layers, etc., will be very much anticipated. The most well-known one is the poor stability of 2D BP in the ambient environment. Although bulk BP is the most stable among all phosphorus allotropes, after processing into few layers, a rapid reaction occurs between the species in air (e.g. oxygen and moisture) and the BP surface, resulting in disruption of the crystal structure. Currently, most of the protective measures explored by researchers are focused on 2D BP in a small area. Such prone to oxidized properties as well as low reliability and repeatability in the wafer-scale BP fabrication process are crucial issues that must be addressed before promoting them into electronic and photonic components. Consequently, addressing these challenges is an important step for BP nanomaterials to be applied in the high-performance devices used for information technology.

Acknowledgement

This work was supported by the grants from National Natural Science Foundation of China (No. 51972279), Research Grants Council of Hong Kong GRF No. PolyU 15301121, AoE/P-701/20, and PolyU Distinguished Postdoctoral Fellowship Scheme (1-YWBG).

References

[1] K.S. Novoselov, A.K. Geim, S.V. Morozov, D.E. Jiang, Y. Zhang, S.V. Dubonos, I.V. Grigorieva, and A.A. Firsov, science **306**, 666-669 (2004).

[2] S. J. Kim, K. Choi, B. Lee, Y. Kim, and B. H. Hong, Annu. Rev. Mater. Res. **45**, 63-84 (2015).

[3] C. Anichini, W. Czepa, D. Pakulski, A. Aliprandi, A. Ciesielski, and P. Samorì, Chem. Soc. Rev. **47**, 4860-4908 (2018).

[4] R. Ding, Y. Lyu, Z. Wu, F. Guo, W.F. Io, S.Y. Pang, Y. Zhao, J. Mao, M.C. Wong, and J. Hao, Adv. Mater. **3**, 2101263 (2021).

[5] X. Cai, Y. Luo, B. Liu, and H.-M. Cheng, Chem. Soc. Rev. **47**, 6224–6266 (2018).

[6] W. F. Io, S. Yuan, S. Y. Pang, L. W. Wong, J. Zhao, and J. Hao, Nano Res. **13**, 1–6 (2020).

[7] S. Y. Pang, W. F. Io, and J. Hao, Adv. Sci. **8**, 2102207 (2021).

[8] S. Y. Pang, W. F. Io, L. Wong, J. Zhao, and J. Hao, Adv. Sci. **7**, 1903680 (2020).

[9] P. W. Bridgman, J. Am. Chem. Soc. **36**, 1344–1363 (1914).

[10] L. Li, Y. Yu, G. J. Ye, Q. Ge, X. Ou, H. Wu, D. Feng, X. H. Chen, and Y. Zhang, Nat. Nanotechnol. **9**, 372–377 (2014).

[11] J.-H. Chen, C. Jang, S. Xiao, M. Ishigami, and M. S. Fuhrer, Nat. Nanotechnol. **3**, 206–209 (2008).

[12] D. Geng and H. Y. Yang, Adv. Mater. **30**, 1800865 (2018).

[13] K. F. Mak and J. Shan, Nat. Photonics **10**, 216–226 (2016).

[14] I. Meric, M. Y. Han, A. F. Young, B. Ozyilmaz, P. Kim, and K. L. Shepard, Nat. Nanotechnol. **3**, 654–659 (2008).

[15] S. Susarla, A. Kutana, J.A. Hachtel, V. Kochat, A. Apte, R. Vajtai, J. C. Idrobo, B. I. Yakobson, C. S. Tiwary, and P. M. Ajayan, Adv. Mater. **29**, 1702457 (2017).

[16] A. Ramasubramaniam, D. Naveh, and E. Towe, Phys. Rev. B **84**, 205325 (2011).

[17] T. Low, A. S. Rodin, A. Carvalho, Y. Jiang, H. Wang, F. Xia, and A. C. Neto, Phys. Rev. B **90**, 75434 (2014).

[18] R. W. Keyes, Phys. Rev. **92**, 580 (1953).

[19] L. Li, J. Kim, C. Jin, G. J. Ye, D. Y. Qiu, F. H. Da Jornada, Z. Shi, L. Chen, Z. Zhang, F. Yang and K. Watanabe, Nat. Nanotechnol. **12**, 21–25 (2017).

[20] N.S. Azar, J. Bullock, S. Balendhran, H. Kim, A. Javey, and K.B. Crozier, ACS Photonics **8**, 1120-1128 (2021).

[21] P.V. Shinde, A. Kumar, D.J. Late, and C.S. Rout , Journal of Materials Chemistry C, **9**, 3773-3794 (2021).

[22] J. Miao, L. Zhang, and C. Wang, 2D Mater. **6**, 32003 (2019).

[23] H. Liu, K. Hu, D. Yan, R. Chen, Y. Zou, H. Liu, and S. Wang, Adv. Mater. **30**, 1800295 (2018).

[24] M. Luo, T. Fan, Y. Zhou, H. Zhang, and L. Mei, Adv. Funct. Mater. **29**, 1808306 (2019).

[25] M. Zhang, Q. Wu, F. Zhang, L. Chen, X. Jin, Y. Hu, Z. Zheng, and H. Zhang, Adv. Opt. Mater. **7**, 1800224 (2019).

[26] G. Qu, T. Xia, W. Zhou, X. Zhang, H. Zhang, L. Hu, J. Shi, X. Yu, and G. Jiang,. Chemical reviews **120**, 2288-2346 (2020)

[27] T. Yin, L. Long, X. Tang, M. Qiu , W. Liang , R. Cao , Q. Zhang, D. Wang, and H.

Zhang, Adv. Sci. **7**, 2001431 (2020).

[28] Z. Wu, W. Jie, Z. Yang, and J. Hao, Mater. Today Nano **12**, 100092, (2020).

[29] F. Bachhuber, J. von Appen, R. Dronskowski, P. Schmidt, T. Nilges, A. Pfitzner, and R. Weihrich , Angew. Chemie Int. Ed. **53**, 11629–11633 (2014).

[30] R. Gusmao, Z. Sofer, and M. Pumera, Angew. Chemie Int. Ed. **56**, 8052–8072, (2017).

[31] L. Pauling and M. Simonetta, J. Chem. Phys. **20**, 29–34 (1952).

[32] N. N. Greenwood and A. Earnshaw, Chemistry of the Elements. Elsevier (2012).

[33] T. Ahmed, M. Tahir, M.X. Low, Y. Ren, S. A. Tawfik, E. L. Mayes, S. Kuriakose, S. Nawaz, M. J. Spencer, H. Chen, and M. Bhaskaran, Adv. Mater. **33**, 2004207 (2021).

[34] Q. Guo, A. Pospischil, M. Bhuiyan, H. Jiang, H. Tian, D. Farmer, B. Deng, C. Li, S.J. Han, H. Wang, and Q. Xia, Nano Lett. **16**, 4648–4655 (2016).

[35] J. Miao, L. Cai, S. Zhang, J. Nah, J. Yeom, and C. Wang, ACS Appl. Mater. Interfaces. **9**, 10019–10026 (2017).

[36] Z. Wu, Y. Lyu, Y. Zhang, R. Ding, B. Zheng, Z. Yang, S. P. Lau, X. H. Chen, and J. Hao, Nat. Mater. **20**, 1203–1209 (2021).

[37] L. Bai, L. Sun, Y. Wang, Z. Liu, Q. Gao, H. Xiang, H. Xie, and Y. Zhao, J. Mater. Chem. A **5**, 8280–8286 (2017).

[38] C. Lin, R. Grassi, T. Low, and A. S. Helmy, Nano Lett. **16**, 1683–1689, (2016).

[39] M. Zhu, S. Kim, L. Mao, M. Fujitsuka, J. Zhang, X. Wang, and T. Majima, J. Am. Chem. Soc. **139**, 13234–13242 (2017).

[40] J. Wang, A. Rousseau, M. Yang, T. Low, S. Francoeur, and S. Kéna-Cohen, Nano Lett. **20**, 3651–3655 (2020).

[41] A. Morita, Appl. Phys. A **39**, 227–242 (1986).

[42] Y. Takao, H. Asahina, and A. Morita, J. Phys. Soc. Japan **50**, 3362–3369 (1981).

[43] A. Castellanos-Gomez, L. Vicarelli, E. Prada, J. O. Island, K. L. Narasimha-Acharya,

S. I. Blanter, D. J. Groenendijk, M. Buscema, G. A. Steele, J.V. Alvarez, and H.W. Zandbergen, 2D Mater. **1**, 25001 (2014) .

[44] L. Liang, J. Wang, W. Lin, B. G. Sumpter, V. Meunier, and M. Pan, Nano Lett. **14**, 6400–6406 (2014).

[45] H. Liu, A. T. Neal, Z. Zhu, Z. Luo, X. Xu, D. Tománek, and P. D. Ye, ACS Nano **8**, 4033–4041 (2014).

[46] Y. Li, S. Yang, and J. Li, J. Phys. Chem. C **118**, 23970–23976 (2014).

[47] Z. Wu and J. Hao, npj 2D Mater. Appl. **4**, 1–13 (2020).

[48] F. Xia, H. Wang, and Y. Jia, Nat. Commun. **5**, 1–6 (2014).

[49] J. Qiao, X. Kong, Z.-X. Hu, F. Yang, and W. Ji, Nat. Commun. **5**, 1–7 (2014).

[50] S. P. Koenig, R. A. Doganov, H. Schmidt, A. H. Castro Neto, and B. Özyilmaz, Appl. Phys. Lett. **104**, no. 10, p. 103106, 2014.

[51] X. Ge, Z. Xia, and S. Guo, Adv. Funct. Mater. **29**, 1900318 (2019).

[52] J. Kim, S. S. Baik, S. H. Ryu, Y. Sohn, S. Park, B.G. Park, J. Denlinger, Y. Yi, H. J. Choi, and K. S. Kim, Science **349**, 723–726 (2015).

[53] J. He, D. He, Y. Wang, Q. Cui, M. Z. Bellus, H. Y. Chiu, and H. Zhao, ACS Nano **9**, 6436–6442 (2015).

[54] X. Liu, J. D. Wood, K.-S. Chen, E. Cho, and M. C. Hersam, J. Phys. Chem. Lett. **6**, 773–778 (2015).

[55] W. Luo, R. Yang, J. Liu, Y. Zhao, W. Zhu, and G. M. Xia, Nanotechnology **28**, 285301 (2017).

[56] S. Fan, H. Hei, C. An, W. Pang, D. Zhang, X. Hu, S. Wu, and J. Liu, J. Mater. Chem. C **5**, 10638–10644 (2017).

[57] S. Yang, A. Kim, J. Park, H. Kwon, P. T. Lanh, S. Hong, K. J. Kim, and J. W. Kim, Appl. Surf. Sci. **457**, 773–779 (2018).

[58] W. Lu, H. Nan, J. Hong, Y. Chen, C. Zhu, Z. Liang, X. Ma, Z. Ni, C. Jin, and Z. Zhang, Nano Res. **7**, 853–859 (2014).

[59] J. Jia, S. K. Jang, S. Lai, J. Xu, Y. J. Choi, J. H. Park, and S. Lee, ACS Nano **9**, 8729–8736 (2015).

[60] G. Lee, J.-Y. Lee, G.-H. Lee, and J. Kim, J. Mater. Chem. C **4**, 6234–6239 (2016).

[61] S. Kuriakose, T. Ahmed, S. Balendhran, G. E. Collis, V. Bansal, I. Aharonovich, S. Sriram, M. Bhaskaran, and S. Walia, Appl. Mater. Today **12**, 244–249 (2018).

[62] M. Akhtar, G. Anderson, R. Zhao, A. Alruqi, J. E. Mroczkowska, G. Sumanasekera, and J. B. Jasinski, npj 2D Mater. Appl. **1**, 1–13 (2017).

[63] S. Kim, Y. Jung, J.-Y. Lee, G.-H. Lee, and J. Kim, Nano Res. **9**, 3056–3065 (2016).

[64] H. Kwon, S. W. Seo, T. G. Kim, E. S. Lee, P. T. Lanh, S. Yang, S. Ryu, and J. W. Kim, ACS Nano **10**, 8723–8731 (2016).

[65] J. Lu, J. Wu, A. Carvalho, A. Ziletti, H. Liu, J. Tan, Y. Chen, A. H. Castro Neto, B. Ozyilmaz, and C. H. Sow, ACS Nano **9**, 10411–10421 (2015).

[66] A. Kundu, R. Rani, and K. S. Hazra, Nanoscale **11**, 16245–16252 (2019).

[67] R. B. Jacobs, J. Chem. Phys. **5**, 945–953 (1937).

[68] M. Köpf, N. Eckstein, D. Pfister, C. Grotz, I. Krüger, M. Greiwe, T. Hansen, H. Kohlmann, and T. Nilges, J. Cryst. Growth **405**, 6–10 (2014).

[69] X. Li, B. Deng, X. Wang, S. Chen, M. Vaisman, S. I. Karato, G. Pan, M. L. Lee, J. Cha, H. Wang, and F. Xia, 2D Mater. **2**, 31002, (2015).

[70] G. Zhao, T. Wang, Y. Shao, Y. Wu, B. Huang, and X. Hao, Small **13**, 1602243 (2017).

[71] C. Li, Y. Wu, B. Deng, Y. Xie, Q. Guo, S. Yuan, X. Chen, M. Bhuiyan, Z. Wu, K. Watanabe, and T. Taniguchi, Adv. Mater. **30**, 1703748 (2018).

[72] N. Izquierdo, J. C. Myers, N. C. A. Seaton, S. K. Pandey, and S. A. Campbell, ACS Nano **13**, 7091–7099 (2019).

[73] D. Han, Q. Liu, Q. Zhang, J. Ji, S. Sang, and B. Xu, Nanoscale **12**, 24429–24436 (2020).

[74] N. R. Glavin, R. Rao, V. Varshney, E. Bianco, A. Apte, A. Roy, E. Ringe, and P. M. Ajayan, Adv. Mater. **32**, 1904302 (2020).

[75] R. Frisenda, E. Navarro-Moratalla, P. Gant, D. P. De Lara, P. Jarillo-Herrero, R. V. Gorbachev, and A. Castellanos-Gomez, Chem. Soc. Rev. **47**, 53–68 (2018).

[76] A. Zavabeti, A. Jannat, L. Zhong, A. A. Haidry, Z. Yao, and J. Z. Ou, Nano-Micro Lett. **12**, 1–34 (2020).

[77] J. D. Yao, Z. Q. Zheng, and G. W. Yang, Prog. Mater. Sci., **106**, 100573, (2019).

[78] L. Lin, B. Deng, J. Sun, H. Peng, and Z. Liu, Chem. Rev. **118**, 9281–9343 (2018).

[79] Y. Shi, H. Li, and L.-J. Li, Chem. Soc. Rev. **44**, 2744–2756, (2015).

[80] J. Zhang, F. Wang, V. B. Shenoy, M. Tang, and J. Lou, Mater. Today **40**, 132–139, (2020).

[81] Y. Xu, X. Shi, Y. Zhang, H. Zhang, Q. Zhang, Z. Huang, X. Xu, J. Guo, H. Zhang, L. Sun, and Z. Zeng, Nat. Commun. **11**, 1–8, (2020).

[82] Z. Yang, Z. Wu, Y. Lyu, and J. Hao, InfoMat **1**, 98–107 (2019).

[83] Z. Yang, W. Jie, C. H. Mak, S. Lin, H. Lin, X. Yang, F. Yan, S. P. Lau, and J. Hao, ACS Nano **11**, 4225–4236 (2017).

[84] G. Bai, Z. Yang, H. Lin, W. Jie, and J. Hao, Nanoscale **10**, 9261–9267 (2018).

[85] Z. Yang, J. Hao, S. Yuan, S. Lin, H. M. Yau, J. Dai, and S. P. Lau, Adv. Mater. **27**, 3748–3754 (2015).

[86] E. S. M. Goh, T. P. Chen, C. Q. Sun, and Y. C. Liu, J. Appl. Phys. **107**, 24305 (2010).

[87] Z. Yang, J. Hao, and S. P. Lau, J. Appl. Phys. **127**, 220901 (2020).

[88] L. Jiao, W. Jie, Z. Yang, Y. Wang, Z. Chen, X. Zhang, W. Tang, Z. Wu, and J. Hao, J. Mater. Chem. C **7**, 2522–2529 (2019).

[89] Z. Yang and J. Hao, J. Mater. Chem. C **4**, 8859–8878 (2016).

[90] P. Yasaei, B. Kumar, , T. Foroozan, C. Wang, M. Asadi, D. Tuschel, J. E. Indacochea, R. F. Klie, and A. Salehi‐Khojin, Adv. Mater. **27**, 1887–1892 (2015).

[91] J. Kang, J. D. Wood, S. A. Wells, J. H. Lee, X. Liu, K. S. Chen, and M. C. Hersam, ACS Nano **9**, 3596–3604 (2015).

[92] P. Chen, N. Li, X. Chen, W.-J. Ong, and X. Zhao, 2D Mater. **5**, 14002 (2017).